Applied Surface Science 672 (2024) 160808

Contents lists available at ScienceDirect

Applied Surface Science

journal homepage: www.elsevier.com/locate/apsusc

Full Length Article

Correlation analysis in X-ray photoemission spectroscopy

Prajna Bhatt [a], Mark Isaacs [a,b], Yuhan Liu [a], Robert G. Palgrave [a,b,*]

[a] Department of Chemistry, University College London, 20 Gordon St, London WC1H 0AJ, UK
[b] HarwellXPS, Research Complex at Harwell, Rutherford Appleton Labs, Didcot OX11 0DE, UK

ARTICLE INFO

Keywords:
XPS
Polymers
Correlation

ABSTRACT

X-ray photoelectron spectroscopy (XPS) is a powerful technique for surface analysis, but its application can be hindered by uncertainty in modelling spectra. Often, many spectral models have a similar goodness of fit, and distinguishing between them can be impossible without additional information. A further challenge is found in interpreting spectra from samples consisting of multiple chemical compounds. We show here how correlation analysis can be used to interpret large XPS datasets. Correlations in atomic concentrations and binding energies of core lines can be interpreted within a framework of an underlying chemical model and this can yield additional information compared with analysis of each spectrum individually. We give examples of the usage of this analysis on some simple systems, and discuss the potential and limitations of the technique.

1. Introduction

The use of X-ray Photoelectron Spectroscopy (XPS) for materials analysis is now well established. As a surface sensitive technique, XPS is able to provide chemical and compositional information that is difficult or impossible to obtain through other methods [1]. When combined with complementary techniques such as Ar^+ ion depth profiling, Raman spectroscopy, Reflectance Electron Energy Loss Spectroscopy (REELS), scanning probe microscopy, diffraction methods, Ion Scattering Spectroscopy (ISS) and others, XPS forms part of a powerful multi-technique platform increasingly used in advanced materials science research [2].

XPS provides quantitative compositional information by comparing the intensities of photoemission peaks from different elements. Additionally, chemical state information can be obtained by measuring the binding energy of core lines [3]. The chemical shift in binding energy between different chemical environments of the same element can be small compared with the peak width. This means individual chemical environments are often not resolved, and peak modelling is needed to determine their binding energies and concentrations. A peak model is the combination of a background function and one or more synthetic peak functions (often of Gaussian-Lorentzian form). Fitting such a peak model to experimental data by varying some of the model parameters to minimise the residual is known as peak fitting [4]. This kind of data analysis plays a major role in the interpretation of XPS spectra [5]. As has been highlighted recently, there are many possible pitfalls in peak fitting, and it is unfortunately common in the scientific literature for conclusions to be stated that are not properly supported by the experimental XPS data [6,7].

A good XPS peak model in materials analysis requires three things:

1. A good fit to the experimental data. This can be measured by statistical methods or assessed by eye (or maybe in future with Artificial Intelligence).
2. To be consistent with spectroscopic theory. Peak shapes, peak widths, peak positions, and background functions should be in accordance with physical theory that describes the photoemission process, and the instrumental parameters of the spectrometer. In some cases it is impractical to physically account for all photoemission processes – for example, background functions account for inelastic emission of electrons, but this kind of emission is often too complex to model and so accepted practice is to employ simple empirical background functions.
3. To be consistent with chemical theory. The model should reflect an underlying, coherent, chemical description of the sample, one that conforms to known chemical laws.

Point 1 is the easiest to achieve in isolation, as a peak model can be made to fit arbitrarily well to any data by simply adding more parameters to the model. A model that meets point 1 but neither points 2 nor 3 is unfortunately not rare in the published literature, but is clearly not able to support any scientific conclusions about the sample.

Point 2 requires knowledge of the physical processes that occur

* Corresponding author at: Department of Chemistry, University College London, 20 Gordon St, London WC1H 0AJ, UK.
E-mail address: r.palgrave@ucl.ac.uk (R.G. Palgrave).

https://doi.org/10.1016/j.apsusc.2024.160808
Received 10 April 2024; Received in revised form 11 July 2024; Accepted 22 July 2024
Available online 23 July 2024

during photoemission spectroscopy. Peak widths, shapes and binding energies are typically interpreted based on physical theory, for example, contributions to the peak width include the lifetime of the core hole created by photoemission, and the vibrational properties of the emitting atoms [8]. Spin orbit coupling affects photoemission according to the properties of atomic orbitals. The background is due to inelastically scattered photoelectrons and secondary electrons. Binding energy shifts can be understood by initial and final state considerations [9]. Energy loss features can be caused by valence electron rearrangement [10]. Instrumental parameters influence observed peak width, and can introduce satellites. Sample treatment, such as sputtering, can introduce artifacts or change the measured chemical composition. Each of these factors, and more, should be considered when constructing a model and assigning features to specific atoms in specific chemical environments. The majority of XPS analysis work in the literature at least attempts to build models consistent with spectroscopic theory. However, even when this point is well implemented, there may still be many different models that fit a particular spectrum or set of spectra equally or nearly equally well. For example, symmetric or almost symmetric spectra can be fitted with a wide range of two component models with almost equal goodness of fit. These models might lead the analyst to similar conclusions, but it can certainly be the case the different models may each fulfil points 1 and 2 while leading to completely different conclusions about the sample in question.

Point 3 is the most often overlooked in material analysis by XPS. In all practical cases, samples are composed of atoms in certain ratios as described by chemical laws. Consistency with chemical theory means that the overall conclusions of the analysis should agree with an underlying chemical model. For example, if a component of the C 1 *s* core line is identified as belonging to a $-CF_3$ group, there should be a F 1 *s* environment with the same assignment, and that F 1 *s* environment should be in a 3:1 concentration ratio with the C 1 *s* environment. Introducing underlying chemical models into XPS fitting provides an additional method to distinguish otherwise similar peak models that may meet points 1 and 2 equally well. It is important to note that the surface chemistry present in the low pressure conditions of a typical XPS measurement may differ from the bulk chemistry under standard conditions.

Several approaches have been advocated to improve confidence in a peak model. Chemical informatics have been increasingly applied to XPS spectra, making use of advanced statistical methods, principal component analysis, multivariate curve resolution, and cluster analysis [11,12]. A related method is use of Bayesian estimation to fit complex core lines [13]. Computational methods can be used to calculate the energies of core lines of different environments which can greatly aid assignment of experimental spectra [14–17]. Fitting over multiple spectra simultaneously can greatly increase confidence in a fit [18], and this is an avenue we explore further in this work.

Here we propose a simple method to interpret XPS data from large datasets, especially from those samples that contain multiple compounds, surface contamination or surface oxidation. It is based on a method used to determine the ratios of intensities two known compounds, described in detail by AG Shard [5]. In that method, a surface known to consist of varying proportions of two phases is measured at several points, and the correlation between intensities of the measured features used to determine the relative intensity ratios of the pure phases. Here we extend this method for use in a wide range of systems. Our analysis relies not on advanced statistical analysis but on underlying chemical models, which we term *phase models*, applying the laws of chemistry to better understand XPS spectra.

2. Correlation analysis

We introduce here the concept of correlation analysis for XPS data. Correlation analysis in general is an established statistical procedure for revealing relationships (which may be causal or coincidental) between variables [19]. The first variable we suggest for correlation analysis in XPS is the concentration of elements, or individual chemical environments of elements, usually measured in relative atomic % (rel. at. %). Element concentration is obtained from core line peak area scaled using relative sensitivity factors that are well established for the most common excitation energies [20,21]. To understand, explain and predict the correlations that may occur in XPS datasets, we use a model of the phase composition of the system. A chemical compound is defined by the ratio of elements it contains, and so we would expect to find particular correlations in the rel. at. % values we measure in XPS between elements or chemical environments present in the same phase. In general, we use the term '*phase*' for a part of the sample with fixed elemental composition. A phase may be molecular or non-molecular, and may consist of one element or many. The sample itself may consist of one phase or several. We describe a proposed set of phases present in a sample as the '*phase model*'. The amount of each phase present can vary, and this is given by the phase fractions, which sum to unity: X_A, X_B, X_C would be the phase fractions of phases A, B and C, respectively.

The second variable we suggest to undergo correlation analysis is binding energy (BE). Despite very common reliance on absolute (or carbon corrected) binding energies for identification of chemical environments, such absolute BEs are difficult to measure reliably due to issues such as charging, and deficiencies of using internal standards such as adventitious carbon are well known [22,23]. However, BE differences between spectral features can usually be measured reliably on a well calibrated spectrometer, if both features have sufficient intensity. From the early days of XPS analysis, it was suggested that binding energy differences between core lines from functional groups could be used to identify such groups [24]. More recent theoretical calculations can give the expected BE differences between functional groups in organic molecules [17]. Here we develop this idea further, and apply to both organic and inorganic materials. We plot correlation graphs of absolute BEs of different spectral features against one another, and relate these correlations to phase models.

Binding energy shifts in XPS can be caused by several factors. The most ubiquitous is sample charging. The build-up of a surface potential on a sample during photoemission is well studied, and it is known that different components of the sample can exhibit different amounts of charging under the same conditions, depending on factors such as their conductivity and morphology [25,26]. For example, metallic samples grounded to the spectrometer typically show almost zero surface potential, whereas insulators can show steady state potentials of tens of volts. Surface potential leads to shifts in the measured binding energy.

A second way that BE shifts can occur in semiconductors is by a change of the Fermi level. Unlike metals, the Fermi level can be altered by several electronvolts in many semiconductors through relatively minor changes in the defect chemistry [27–29]. Fermi level shifts cause the measured binding energy of core lines to shift by an equivalent energy.

We can now consider the effects of these forms of BE shift from the perspective of the chemical phase model of a sample. Core lines arising from atoms in the same phase will be expected to experience the same BE shift due to charging, as long as the surface potential is homogeneous on the atomic scale. Since the conductivity is a property of the material as a whole, not the individual atoms that make it up, this is a reasonable assumption. Likewise, the BE changes due to Fermi level shift can be thought of as applying to all atoms within a phase equally. The conclusion is that in the absence of major chemical changes to a phase (e.g. significant oxidation or reduction), the chemical environments that are together in the same phase will undergo BE shift of the same amount by charging and by Fermi level changes, that is, they will exhibit a constant BE difference. Therefore, we would expect the absolute BEs of chemical environments in the same phase to show a linear correlation with a gradient close to one. We use this to identify chemical environments that may be in the same phase.

Examples of both atomic % correlations and BE correlations will be

given in the sections that follow. For correlation analysis to be effective, many individual sets of XPS spectra on the same or related samples are needed. There are several ways to achieve this. For example, a depth profile is typically carried out by recording spectra, etching the sample, and repeating this process for many cycles. This results in a collection of many sets of spectra (each set being the different core lines and, in some cases, survey). XPS mapping over a large sample, where many sets of spectra are recorded at different points may also be suitable, as will measurement of many samples of the same type or collection of data on the same sample at different pressures or with different photon energies. We refer to any such collection comprising of several sets of data as a '*dataset*'.

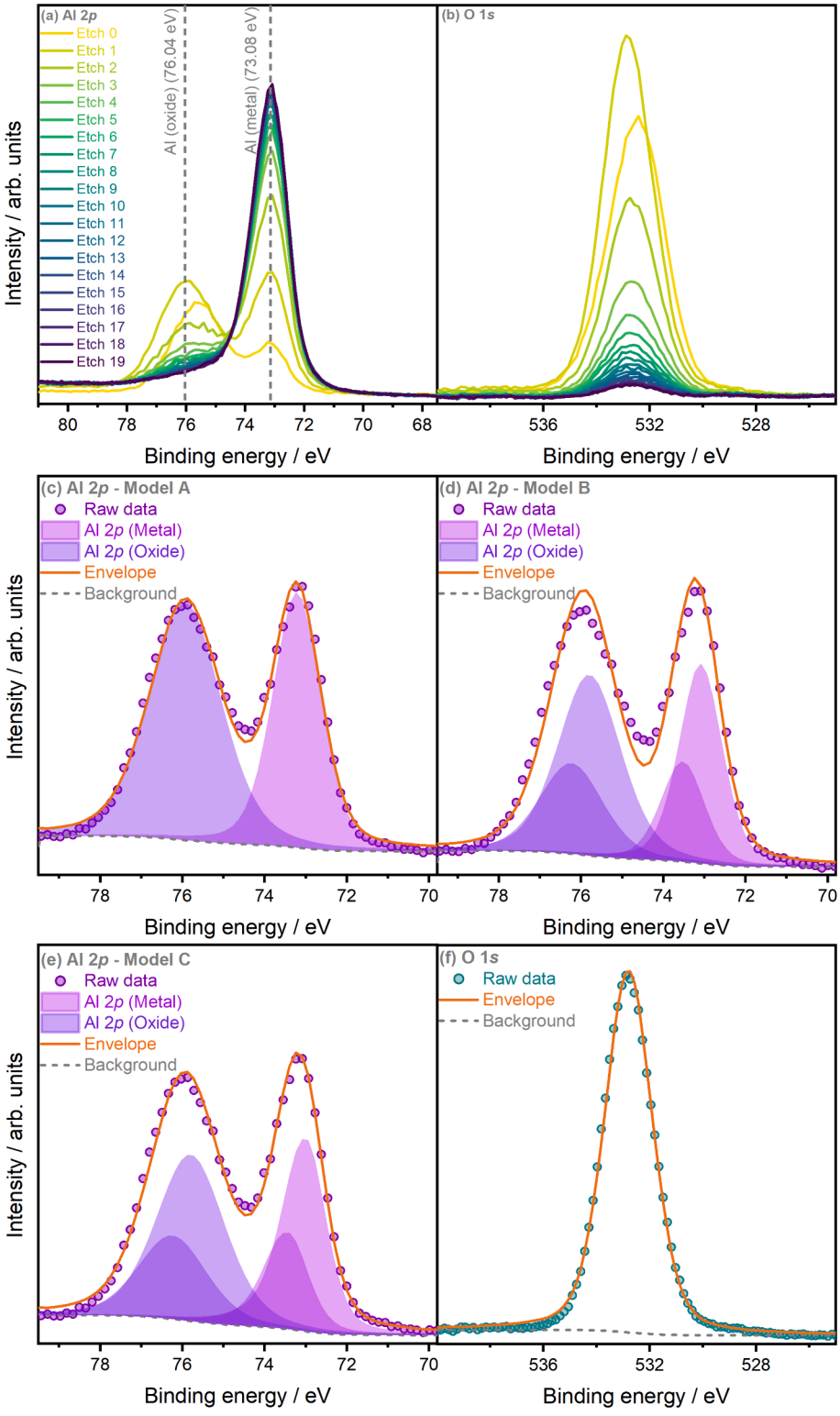

Fig. 1. Spectra from the depth profile of Al foil with a native oxide layer. (a) Al 2*p*, (b) O 1*s*. The three models descried in the text are shown in (c), (d), (e), applied to the same experimental data. The model for the O 1*s* peak shown in (f) was used in all cases.

2.1. Example 1: Aluminium foil native oxide

To illustrate the concepts discussed so far, we introduce the first example: depth profile analysis of aluminium foil with a native oxide layer at the surface. The Al 2*p* and O 1*s* spectra are shown in Fig. 1 (the C 1*s* spectra are shown in Fig. S1). We can have high confidence that our sample in this case will consist of an Al_2O_3 phase representing the oxide layer, and an Al phase representing the bulk of the foil: this is the phase model we will use for this system. The phases Al and Al_2O_3 are said to be isoelemental as they share a common element (Al). On etching the foil using Ar^+ ion etching, we would expect to gradually remove the Al_2O_3 layer. The dataset produced from such a depth profile would consist of sets of spectra with varying proportions of the two phases (Al and Al_2O_3), i.e. different phase fractions, X_{Al} and X_{Al2O3}. If X_{Al2O3} were 100 % (i.e. no Al metal present) then the total at. % of Al would be 40 % and O would be 60 %, according to the formula Al_2O_3. If X_{Al} were 100 %, then clearly the total at. % of Al would be 100 % and that of O would be 0 %. Any mix of the two phases will fall in a line between these two limits, and so in this case the correlation between at. % Al and at. % O for a mixed Al/Al_2O_3 sample is linear with a gradient of −1. Fig. 2(a) shows the experimental correlation plot of at. % compositions between Al and O for the dataset from etching of the native oxide layer on Al foil. The first level, the as-presented surface, contained a significant amount of carbon and this level was excluded from the dataset (Fig. S1). Carbon was however included in the at. % calculation for all levels. Past the first level, the remainder of the experimental data shows the predicted correlation between Al and O at. %, with an experimental gradient of −0.97. This in itself is not surprising, as for any system predominantly made up of two elements, this gradient in their correlation should exist. We can also observe the largest value for the at. % O is around 45 at. %, less than the stochiometric limit of 60 at. % when $X_{Al2O3} = 100$ %.

The above analysis considered the different Al environments together, but it is possible to separate them, since the chemical shift between Al(metal) and Al(oxide) in the Al 2*p* peak is large.

Here we show how correlation analysis can help distinguish between competing models. We use three different models, labelled A, B, C, in increasing order of complexity, to fit the same dataset. All use a Shirley background defined over the same range. Model A consists of two 70 % Gaussian 30 % Lorentzian sum components: one to represent the Al oxide and one to represent the Al metal environments. For each spectrum in the dataset, the FWHM and position is refined. This model represents a naïve approach, deliberately omitting several important features of the physics of photoemission.

Model B uses a spin orbit doublet for both metal and oxide environments. The separation is fixed at 0.44 eV and the intensity ratio at 2:1. A symmetrical Gaussian-Lorentzian sum is used for all components. The FWHM for the oxide and metal environments were individually set using the first and last (most oxide rich and most metal rich) spectra respectively, and this was set for the whole dataset.

Model C is the same as Model B but the Al metal peaks are given asymmetry using an exponential tail on the high BE side, as described by Sherwood [30]. All peak fitting parameters are summarised in detail in Table S1.

The correlation between the Al 2*p* (oxide) and O 1 *s* atomic percentages for each model is shown in Fig. 2(a). The Al 2*p* (oxide) environment should have a positive correlation with the O 1*s* in atomic % with a gradient of 1.5, which reflects the Al_2O_3 stoichiometry, and is indicated by the dashed line in Fig. 2(a). For models A and B, many of the correlation points fall below the expected line. This indicates that the model is higher in Al 2*p* (oxide) concentration than should be expected for a given concentration of oxygen. We also see that the deviation from the expected correlation is greater for lower amounts of oxygen. This suggests that the problem is with the description in models A and B of the Al 2*p* (metal) peak, which is more prevalent when the amount of oxide is low, and so will have a greater impact on the overall fit at low levels of oxygen.

In this case it is clear that improper description of the Al 2*p* (metal) peaks in models A and B means the contribution of the metal peaks to the intensity in the region of the Al 2*p* (oxide) peaks is not properly accounted for. Correcting this, first by adding spin orbit coupling in Model B improves the situation, and finally by adding in asymmetry to the metal peaks (Model C) results in a good match to the expected correlation based on chemistry. We observe gradients of 2.03, 1.94 and 1.57 respectively for models A, B and C respectively for the correlation under discussion, with the expected value being 1.5.

Turning to the correlation between binding energy of spectral features, the correlation plots between the Al 2*p* (oxide) and O 1*s* BEs shown in Fig. 2(b). Since the concentration of Al 2*p* (oxide) falls very low

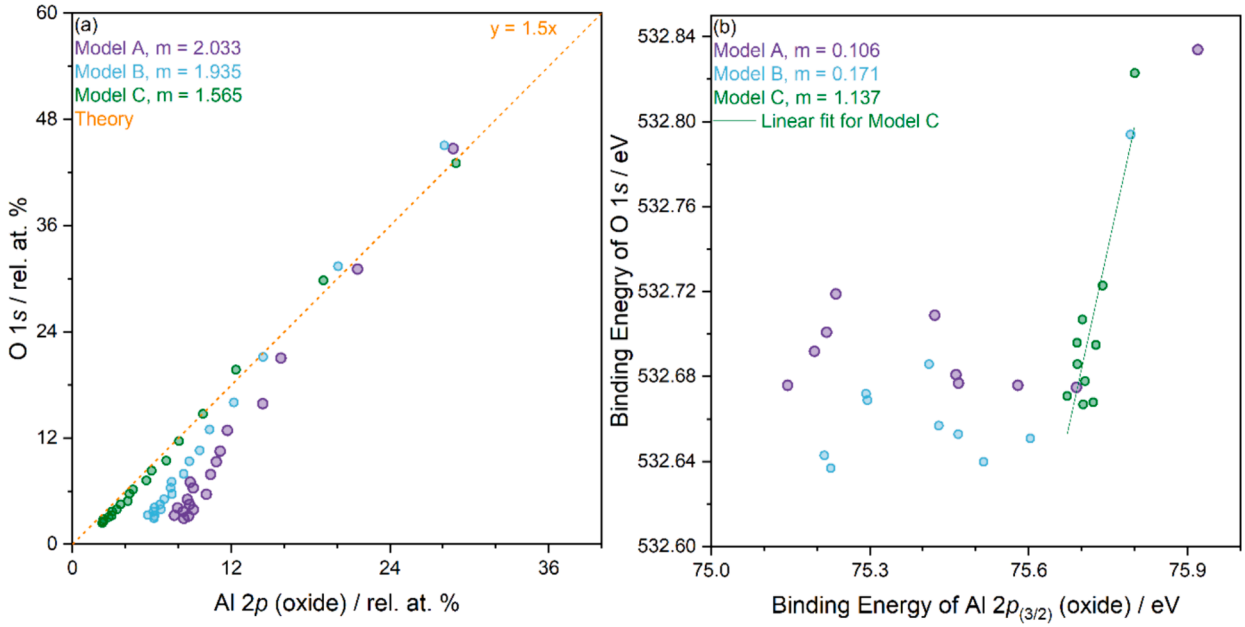

Fig. 2. Correlation plots of experimental dataset from the etching of Al foil with native oxide layer. (a) correlation between Al 2*p* (oxide) and O 1*s* atomic % (b) correlation between Al 2*p* (oxide) and O 1*s* binding energy. The gradient of each linear fit, m, is shown in the legend of each panel.

in later etch levels, leading to large instability in the refined positions of the oxide peaks, only the first 10 levels are considered, where the Al 2*p* (oxide) environment is above 10 at. %. The binding energies of Al 2*p* (oxide) and O 1*s* show no strong correlation for peak models A and B, even in this surface oxide rich region (Fig. 2b). The poor match between the expectations from the phase model, and the correlations produced by the more naïve peak models, might cause the analyst to consider alternatives. Model C, however, gives a roughly linear correlation, with gradient close to 1 (m = 1.14), as expected for chemical environments in the same phase. We note that the Al 2*p* (metal) and C 1*s* peaks show no correlation with the O 1*s* or Al 2*p* (oxide) peaks, again showing they are not in the same phase.

In this way, the three models can be compared based not only on their correspondence to one spectrum, but across a whole dataset, and not only against statistical goodness of fit, but against the fit to the underlying chemical model. Clearly in this case, Model C is superior.

In this example we used a system with a high degree of certainty about the phases present. The native oxide on aluminium foil is well characterised, and only one oxide of aluminium is known. Under these circumstances, we can use the confidence in our phase model to test different *peak models* for their adherence to the *phase model* using correlation analysis.

We will now consider some general features of correlation analysis and the phase model in XPS before further experimental examples.

Firstly, it is clear that to predict correlations in atomic %, a phase model must contain two or more phases, and these phases must be able to vary in phase fraction across the dataset. A one phase model, or a model where the phase fractions are fixed (which is functionally the same as a one phase model from an atomic % correlation point of view), will only ever have one value of concentration of each element by definition, so meaningful correlations beyond this one value will not result. It would still be possible to carry out binding energy correlations to test ideas of which elements belonged to the same phase, in our framework these would be expected to have linear correlations of binding energy with a gradient of 1. But no meaningful concentration correlations would be possible.

The simplest case of a multi-phase model is one where no phases share any common elements – we call such phases anisoelemental (i.e. containing no common elements). In a phase model consisting of two anisoelemental phases, A and B, the at. % correlation of two elements can be understood as follows. First consider two points on the at. % correlation graph that result from phase fractions, X_B=100 %, and X_A=100 %. When X_A=100 %, naturally X_B is zero, and so elements in phase B have zero concentration and the atomic percentages of the elements in Phase A are those present in the pure phase, for example if the elements are in equal stoichiometry in phase A then then each element will be at 50 at. % when X_A=100 %. Any lower value of X_A will result in points along the straight line between the points on the correlation plot representing X_B=100 % and X_A=100 %. We refer to such a line that links the points representing X_A=100 % and X_B=100 % as a 'tie line' for phases A and B, and we refer to this line as $T_{A,B}$.

It follows that in a phase model with only anisoelemental phases, the expected at. % correlation between elements in the same phase will be the tie line – it will always be linear with positive gradient equal to the stoichiometry ratio on the phase, and with an intercept of zero. Elements in different anisoelemental phases A and B will be negatively linearly correlated if there are exactly two phases, and points will lie along the tie line for those phases.

If there are three or more anisoelemental phases then the correlation graph between a pair of elements in different phases, A and B, will have an upper bound of the tie line of phases A and B. Points may exist below $T_{A,B}$ and these represent cases where elements of a third phase makes up some portion of the atomic % of the sample. The practical result is that for three or more anisoelemental phase, and all three phases are present in similar proportion, there can appear to be no correlation between elements in different phases.

2.2. Example 2: Tin oxides

The next consideration is phase models that involve at least some isoelemental phases, i.e. elements that share a common element. In a two-phase system with isoelemental phases A and B (such as the case of Al and Al_2O_3 given above) the at. % correlation graph that includes a shared element will be linear and will fall along the tie line, $T_{A,B}$, for phases A and B. For phase models with three or more phases, correlation graphs for elements in isoelemental phases will be bounded by the tie lines for those phases. This arrangement is illustrated in the following example. Here, we consider a system consisting of two oxides of tin, SnO and SnO_2. We also consider a third phase representing an impurity that contains neither Sn nor O. We label this phase C. The elemental composition of phase C is not important for this discussion, but this could be for example, adventitious carbon or some other impurity.

We consider the atomic % correlation graph between Sn and O. Fig. 3 shows four simulations of this correlation graph for this system. In each case three tie lines are depicted. The purple dashed tie line is $T_{SnO,\ SnO2,}$ this tie line therefore joins the points where X_{SnO}=100 % and X_{SnO2} = 100 %. The orange tie line is $T_{SnO2,\ C}$ and the green tie line is for where $T_{SnO,C}$. The possible values for this phase model for the Sn – O correlation graph are bounded by these three tie lines, and so fall in the triangular areas shown in Fig. 3. We simulate datasets in the phase model by plotting 50 points with randomly determined phase fractions of each of the three phases (SnO, SnO_2 and C). In Fig. 3(a), the random distributions SnO and SnO_2 are equally weighted, with the amount of Phase C weighted three times more highly. The points are evenly distributed throughout the triangular region bounded by the tie lines, with a weak positive correlation between Sn and C atomic %. In Fig. 3 (b), the simulated phase distribution is still random but the SnO phase is given a weighting of 20 times that of SnO_2. This represents a set of samples where SnO is the main Sn containing phase. The points in this simulation lie close to the green tie line, i.e. $T_{SnO,C}$. Fig. 3(c) shows a distribution with a low amount of Phase C, and equally weighted random amounts of SnO and SnO_2. Here the points lie close to the blue tie line ($T_{SnO2,SnO}$), with gradient close to −1, showing that the large proportion of the sample is Sn oxides with minor impurities. Lastly Fig. 3 (d) shows the situation where the SnO weighting in the simulation is 20 times less than that of the SnO_2 phase. The points lie close to the red tie line ($T_{SnO2,C}$), and this is representative of a system where the majority of the Sn present in the system is in a SnO_2 phase. The gradient is close to 2, which comes from the stoichiometry of the SnO_2 phase.

In systems that contain isoelemental phases (such as SnO and SnO_2) in addition to other phases, the correlation between the atomic % of common elements may be weak or non-existent if a significant amount of a third phase is present, as in Fig. 3(a). Thus it is important to note that absence of correlation in the rel. atomic % of elements does not rule out the possibility that those elements exist in the same phases.

Following the consideration of the SnO_2/SnO/C phase model, we now apply this model to an experimental dataset. Our dataset consists of a depth profile of a commercial SnO powder which was oxidised at the surface by heating at 400 °C in air for 1 h. The intention was to create a SnO_2 rich surface, which could then be etched revealing more SnO. The powder was pressed onto carbon tape, and analysed by XPS. Ar^+ ion depth profiling was used to remove the surface layer. Fig. 4 shows the Sn 3*d*, O 1*s* and C 1*s* spectra in this dataset.

First, the total atomic composition for each of the three elements were calculated, without any peak fitting. The correlation between Sn and O at. % is shown in Fig. 5 as the pink circles (total atomic %). It can be seen that some points are outside the tie lines defined earlier for this phase model – at the first and second depth profile levels, where the O: Sn ratio is too high to correspond to any possible mixture of SnO_2 and SnO. This indicates that, assuming there is no previously unknown higher oxide of Sn, that the O 1*s* peak must contain contribution from another oxygen environment. We fit the O 1*s* with two components, a broad higher energy component which is assigned to organic oxygen,

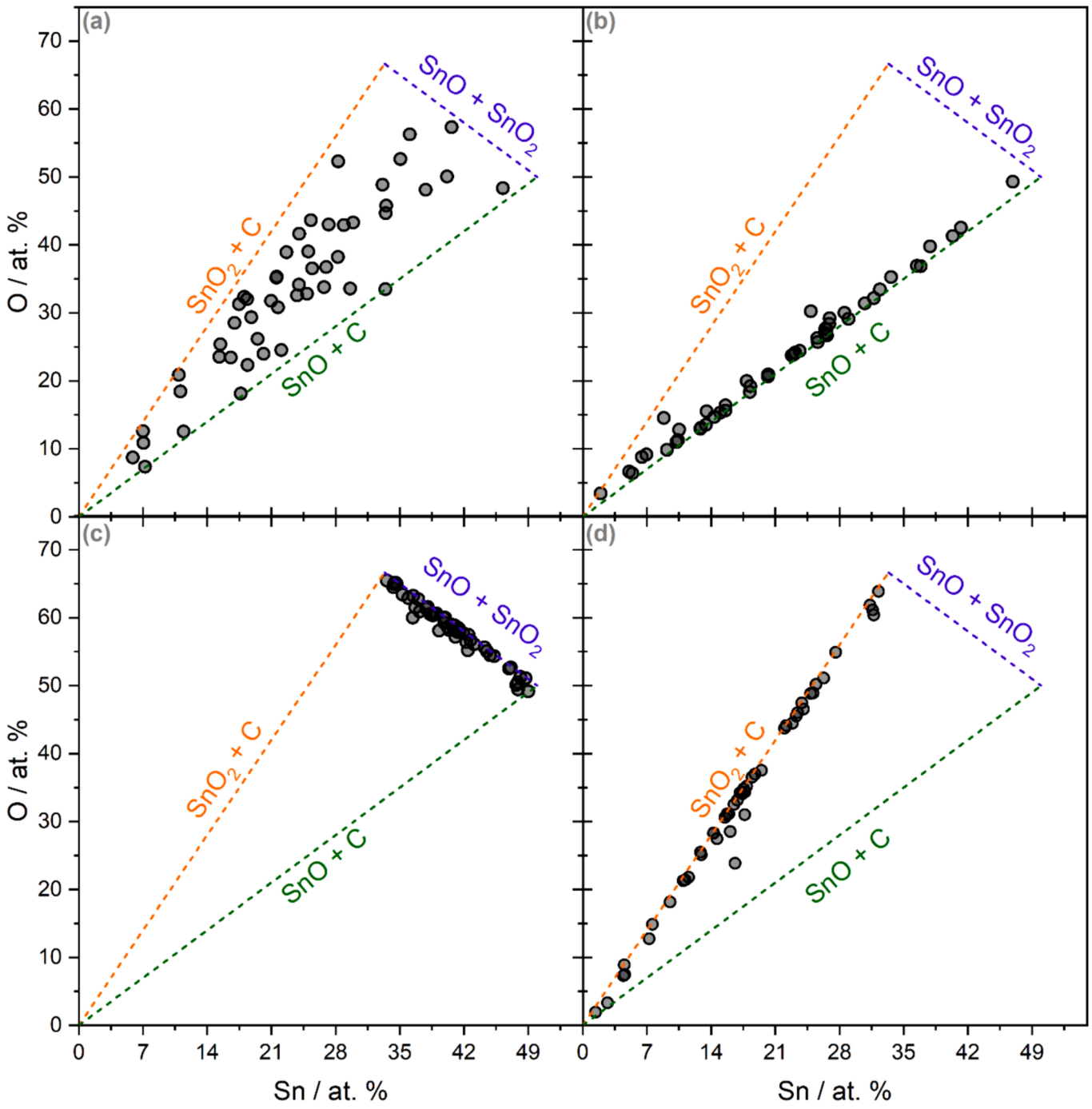

Fig. 3. Atomic % correlation plots between Sn and O for four simulated datasets for SnO_2/SnO/C model. Marked lines are the tie lines between the indicated phases. Each simulated dataset has 50 points with phase compositions randomly determined but weighted differently. (a) A random mixture of all three phases – there is a weak positive correlation between Sn and O atomic %. (b) A mixture of SnO+C, with small amounts of SnO_2. The points lie close to the SnO+C tie line, with a gradient close to 1, the ratio of Sn:O in SnO. (c) A mixture of SnO_2 + SnO, with small amounts of C. The points lie on the SnO+SnO_2 tie line, with gradient close to −1. (d) A mixture of SnO_2 + C, with small amounts of SnO. The points lie on the SnO_2 + C tie line, with gradient close to 2, i.e. the ratio of Sn:O in SnO_2.

present in the surface contamination layer. This component has fixed FWHM of 2.12 eV and a BE that can vary in the between 531–532 eV. The lower binding energy, sharper peak we assign as the oxide environment, in either SnO or SnO_2 (Fig. S3, Table S2). This peak has a fixed FWHM of 1.36 eV. The Sn/O correlation, where only the O 1*s* (oxide) environment is included, is shown as yellow triangles in Fig. 5. As can be seen, adoption of this fitting model moves the correlation plot inside the tie lines, meaning it is consistent with the SnO_2/SnO/C phase model. The order of the datapoints, i.e. from start to end of the depth profile, is indicated by the arrows in Fig. 5. When the O 1*s* fitting model is used, the correlation shows that the surface begins as almost pure SnO_2 + C, with very little contribution from SnO. As the etching proceeds, the amount of contaminant phase C decreases (shown by movement towards the SnO+SnO_2 tie line) and the amount of SnO increases (shown by movement towards the SnO composition, i.e. 1:1 Sn:O). Thus, the changing atomic composition from the dataset can be interpreted as a changing phase composition within the proposed phase model. This gives some confidence that the fitting used to produce this correlation (in this case fitting of the O 1*s* peak to separate organic oxygen) is at least consistent with the phase model proposed, and the expected variation of the phases

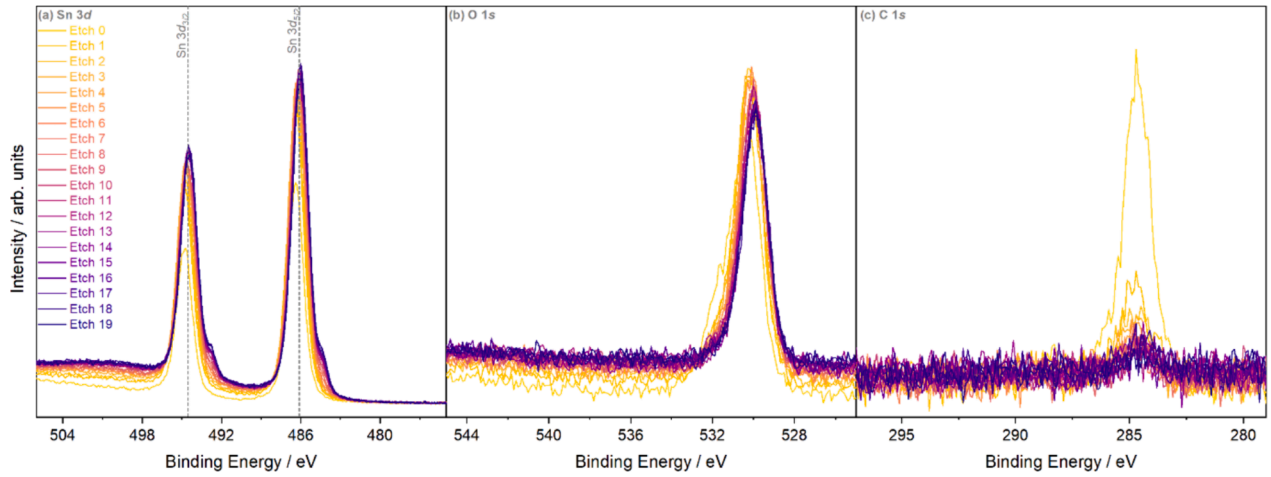

Fig. 4. XPS spectra from depth profile of oxidised SnO powder. (a) Sn 3*d*, (b) O 1*s*, (c) C 1*s*. No charge correction was applied to any spectrum.

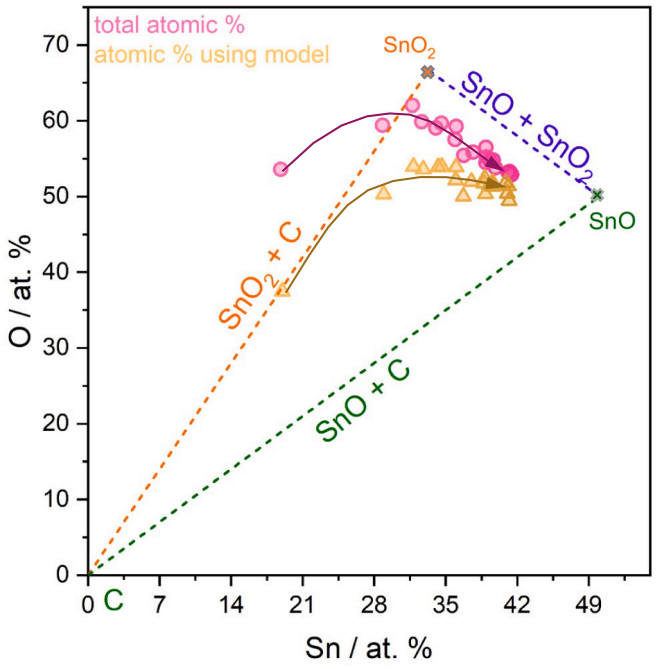

Fig. 5. Atomic % correlation between Sn and O for an experimental dataset. Tie lines relate to the SnO_2/SnO/C model described in the text. Pink circles show datapoints from the total atomic concentrations (without fitting). Yellow triangles show datapoints when the O 1*s* core line is fitted to distinguish organic oxygen and oxide components, with only the oxide components included in the correlation plot. The two crosses show the positions of pure SnO_2 and SnO as labelled. Arrows show the order of the datapoints in each series, from start to end of the depth profile. (For interpretation of the references to colour in this figure legend, the reader is referred to the web version of this article.)

with etching.

Close examination of the Sn 3*d* spectra in Fig. 4 shows the presence of low binding energy peak that grows with etching time. Considering the BE of these features, it is assigned to Sn metal produced by etching damage. The presence of this Sn phase will allow the Sn:O ratio to fall below the SnO+C tie line – i.e. to become more Sn rich than is possible with our phase model. This does not actually occur in our experiment, but with extended etching time it may do. This could be accounted for by addition of a Sn metal phase to the phase model.

Using this method, the phase fraction of SnO, and therefore the average oxidation state of Sn, can be determined at any point in the depth profile. We further studied whether a model of Sn 3*d* peak could be used to separate the Sn(II) and Sn(IV) environments. Unlike in the case of Al_2O_3 and Al above, we found no way to model the Sn 3*d* peak that would separate the chemical environments of Sn and give a result consistent with the average oxidation states determined from our analysis. We therefore agree with the established view taken by previous authors who studied tin oxide XPS, which is that the Sn 3*d* peak has no discernible chemical shift between SnO and SnO_2 [31,32]. Determining the average oxidation state by consideration of the metal to oxygen stoichiometry has been used many times previously, for example In a well-known study of the oxides of vanadium [33]. We believe the framing of this analysis in terms of atomic correlations provides a new viewpoint on this method.

Lastly, we consider the binding energy correlation between elements. Fig. 6(a) shows a linear correlation between the binding energies of the Sn $3d_{5/2}$ and the O 1*s* spectral maxima. The gradient is 0.92, reasonably close to the gradient of 1 expected for elements in the same phase. This adds evidence to the hypothesis that the SnO and SnO_2 environments of both Sn 3*d* and O 1*s* peaks are indistinguishable – i.e. they each behave as one peak and their binding energies are correlated. In contrast, there is no correlation between the BEs of C 1*s* and Sn $3d_{5/2}$ peaks, showing that, as expected, these elements are not in the same phase. The lack of correlation between C 1*s* and any of the other peaks in the sample seems to be an indication that binding energy referencing to C 1*s* is not suitable in this case.

2.3. Example 3: Polymer mix

The final example uses organic polymers. We take a mixture of two polymers and approach this problem from the opposite perspective to the other examples. Previously, we proposed a phase model first and from this built a peak model, to then interpreted correlations in terms of those models, changing one or other of the models if needed to find agreement. Here we first build a peak model, then observe correlations and finally attempt to build a useful phase model. In reality, the identity of the polymers was known to us throughout, but we believe the procedure described here could be used to identify unknown phases in some circumstances.

The sample consisted of inhomogenously mixed powders of the two polymers spread over carbon tape with area of approximately 15 x 5 mm. No special cleaning steps were taken, this was to simulate a more 'realistic' sample in XPS analysis which is likely to contain impurity phases alongside the phases of interest; as we will discuss below, impurity phases played a role in this example, as is likely many real analysis problems. A grid of 121 points was defined over the sample area; survey and high resolution core line spectra were recorded at each

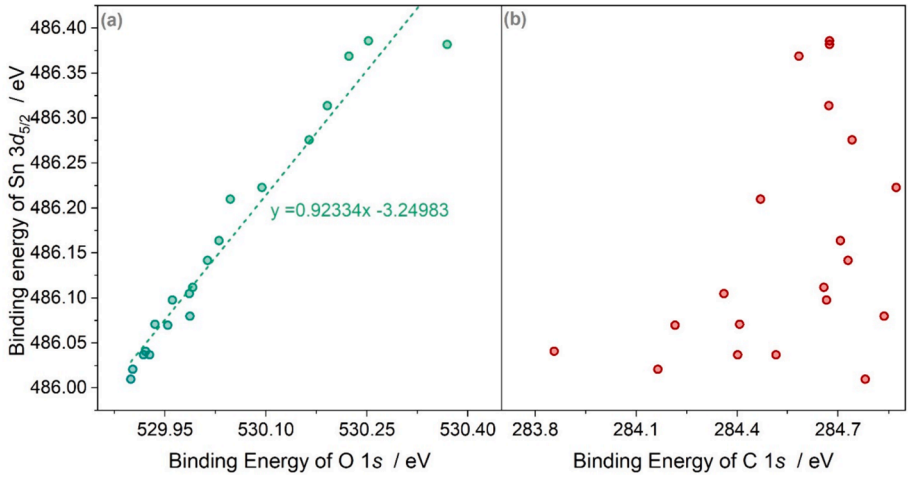

Fig. 6. Binding energy correlation between (a) O 1*s* and Sn $3d_{5/2}$ and (b) C 1*s* and Sn $3d_{5/2}$.

point under the same collection conditions. These spectra together represent the dataset. Initial analysis showed carbon and oxygen, and a small (<5 at. %) amount of silicon. Examination of the C 1*s* and O 1*s* regions suggested that they consisted of multiple overlapping components.

We begin to construct a peak model for the C 1*s* and O 1*s* high resolution spectra as follows. A Shirley background was added across each core line. Two components were added to the model and were constrained to have equal FWHM. No constraints on intensity or position were imposed, and the peak shape was fixed at a 30 % Lorentzian, 70 % Gaussian sum, detailed in Table S3. The model was fitted over all spectra in the dataset. If the model left clearly unfitted intensity, judged by eye rather than statistically, another component was added with the same constraints, and the process repeated. This led to a O 1*s* model with two components, and a C 1*s* model with four components. Components were labelled A,B,C,D with increasing BE.

C 1*s* components were found around 284.5 eV (A), 285.0 eV (B) 286.4 eV (C), and 288.5 eV (D). O 1*s* components were found around 531.7 eV (A) and 533.7 eV (B). Individual components moved by less than 0.8 eV across the whole 121 spectrum dataset. Possible assignments based on the tabulation of Smith et al. [34] are shown in Table 1, and a sample spectrum fitted with this method for each core line is shown in Fig. S4.

Use of an equal FWHM model is not always optimum, but in the absence of any other knowledge of the sample, and for 1*s* spectra, we believe it is an effective starting point. In this case, the result is a total of six different components. An issue we found was that the fitting was unstable in the intensities of the C 1*s* (A) and C 1*s* (B) components, which have BEs ≈ 0.5 eV apart. For C 1*s* spectra of similar shape, the best fit might have very different contributions from C 1*s* (A) and C 1*s* (B), due to the close spacing of these components. This issue complicated the correlation analysis, and so we took the step of summing C 1*s* (A) and C 1*s* (B), considering them as a single component for the purposes of atomic % correlation.

Table 1
Peak model used to fit the mixed polymer sample, alongside possible assignments from Smith et al. [34].

Carbon environment	Possible identity	Oxygen environment	Possible identity
C 1*s* (A) 284.5 eV	C–C–C	O 1 *s* (A) 531.7 eV	C=O
C 1*s* (B) 285.0 eV	Aromatic, C–C-X (X=heteroatom)	O 1 *s* (B) 533.7 eV	C-O aromatic or aliphatic
C 1*s* (C) 286.4 eV	C-O	–	–
C 1*s* (D) 288.5 eV	C=O, O=C-O	–	–

Fig. 7 shows the pairwise % at. concentration correlations between the now five components (as C 1*s* (A) and C 1*s* (B) summed together). The gradients of linear trendlines fitted to these correlations are shown in Table 1.

There are several ways to approach the problem of building a phase model from the correlations shown in Fig. 7. Statistical methods might be used to assess a large number of plausible models against the relationships shown in Fig. 7. Here we take a more chemically intuitive approach that will likely be more flexible for a wider range of situations.

In Fig. 7, panels (a), (c) and (h) show the most strongly linear correlations, which we discuss first. It is immediately noticeable that the correlation between C 1*s* (D) and O 1*s* (A) has a gradient close to unity (Fig. 7 (a), Table 2), consistent with a situation where these two environments are together in the same phase in a 1:1 ratio, and not present in another phase. Looking at the BEs of these environments, 288.6 eV and 531.7 eV for C 1*s* (D) and O 1*s* (A), these correspond to reported values for the elements in a carbonyl group, C=O [34], and that the 1:1 stoichiometry also matches the expected value for that functional group. Thus we place C 1*s* (D) and O 1*s* (A) as a carbonyl group present in only one of the phases. There is also a strong linear correlation between C 1*s* (D) and C 1*s* (A+B) (Fig. 7h). The negative gradient of this correlation shows that the phase containing the carbonyl functional group is less rich in aliphatic/graphitic carbon than the other phase.

The remaining carbon environment is C 1*s* (C). This has a BE of around 286.4 eV, close to that expected for alcohols or ether groups [35]. The C 1*s* (C) concentration shows a positive correlation with C 1*s* (D) environment, but the gradient is far below 1 (the value is + 0.23, Table 2). If the C 1*s* (D) concentration is extrapolated to zero, then approximately 9.0 atomic % of C 1*s* (C) would remain. This shows that unlike the carbonyl group, the C-O environment appears in both phases. This is confirmed with similar analysis on the O 1*s* (B) which seems to be the oxygen counterpart of the C 1*s* (C) environment. O 1*s* (B) appears at 533.7 eV, at the top end of the range for alcohols and ethers, the slightly higher BE for O 1*s* (B) may be due to O bound to an aromatic system or in an ester group [34]. The O 1*s* (B)/C 1*s* (C) pair show a positive correlation with gradient of + 0.75, close to but not exactly 1.

Thus we conclude that both phases contain a C-O group, and only one phase contains a C=O group. The latter is less rich in aliphatic/graphitic carbon. We may continue from here by trialling certain structures, and assessing the predicted correlations against the measured ones. We believe doing so would yield further information on the unknown polymers.

As stated, the polymers were known to us, and were poly(methyl methacrylate) (PMMA) and poly(4-vinylphenol) (PVPh). PMMA and

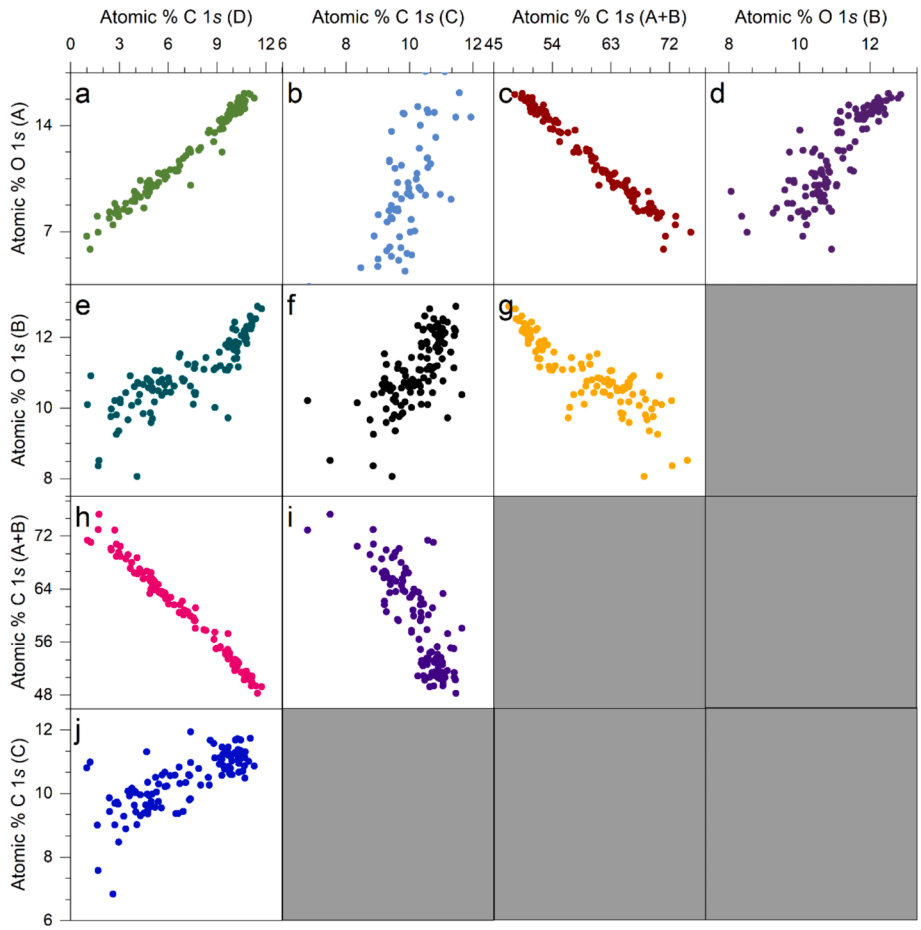

Fig. 7. Correlations between concentrations of the five components of the C 1*s* and O 1*s* regions identified in the polymer mix dataset. The binding energies of each component are stated in the text.

Table 2
Gradients of linear trendlines fitted to the correlation plots of the five environments identified in the polymer mix. The table is arranged in the same was as Fig. 7 and is intended to be read alongside it.

	C 1*s* (D)	C 1*s* (C)	C 1*s* (A+B)	O 1*s* (B)
O 1*s* (A)	+0.94	+2.31	−0.38	+2.34
O 1*s* (B)	+0.29	+0.75	−0.12	
C 1*s* (A+B)	−2.45	−6.5		
C 1*s* (C)	+0.23			

PVPh have both been well studied by XPS and assignments that relate to the four carbon and two oxygen environments can be seen in Supplementary information Fig. S4 [36,37]. PVPh contains an aromatic ring and a OH group, the latter accounting for the C 1*s* (C) and O 1*s* (B) environment in that phase.

Given the known structures of the two polymers, and the assignment of each carbon and oxygen to one of the identified environments, it is possible to calculate the expected gradients of all of the correlations. Theoretical linear gradients were calculated by taking conventional modelling of the two polymers, shown in S4. This phase model leads to the theoretical atomic % and correlation gradients shown in Table S1 and S2.

We can now discuss the successes and failures of the correlation approach in this example. Firstly, we were correctly able to identify functional groups, and to which phase they belonged, by their correlations. The measured gradients for the C 1*s* (A+B) and C 1*s* (C) environments were close to those of the correct phase model. This also allowed us to determine which of the phases had more aliphatic/graphitic carbon.

However, the gradients measured for the correlations involving C 1*s* (C) were far from the theoretical values. This was a challenging component to model because it actually represented two different environments (aromatic alcohol and ester group in the different phases, Fig. S4), it had low intensity and also overlapped with C 1*s* (B). In contrast, C 1*s* (D) correlations were very close to the theoretical values. This was because C 1*s* (D) was not significantly overlapped with another component, so even though its intensity was similar to C 1*s* (C), it was able to be modelled much more accurately across the dataset.

The O 1*s* (B) correlations were also significantly different from the theoretical. This is likely due to the presence of oxygen (and silicon) from the underlying carbon tape in some places in the dataset, which increased the O 1*s* (B) signal anomalously.

Using correlation analysis to build a phase model from scratch, as attempted in this final example, is clearly challenging. Some success was found here through a strategy of identifying the most strongly linear correlations and attempting to identify them, despite sample contamination. Although a complete phase model could not be obtained from this information alone, important insights on functional group identification could be made which would have been much more difficult from the individual spectra in isolation. In most practical cases, some additional information will be known about the sample and this may be used to improve the phase model.

3. Conclusions

We present a simple method of correlation analysis in XPS. This method seeks to identify correlations between both atomic

concentration and binding energies of different species across large datasets. These correlations are then understood on the basis of a phase model: a description of the chemical compounds present in the sample.

This method can be used in several ways:

Firstly, if a likely phase model is known for the system under investigation, then correlation analysis can be used to test whether XPS peak fitting is consistent with that phase model, and to assess competing peak models against each other, based not only on statistical measures of goodness of fit but also fit to a coherent chemical model. In our examples of the depth profiling of Al foil, which is well known to have a native oxide layer. Use of both the total Al concentration, as well as fitting to distinguish Al(III) and Al(0), agreed closely with the predicted correlations, and the superiority of one peak fitting model over the other was clear.

Secondly, once a phase model is accepted, then a dataset can be interpreted in terms of phase fractions rather than atomic % of individual elements. We showed the use of this with the SnO/SnO_2 system, where phase fractions, and hence average Sn oxidation states, for each level could be obtained, even though the Sn 3*d* peak cannot be successfully fitted with Sn(II) and Sn(IV) components. By considering the range of possible Sn:O correlations, we identified that the surface consisted of an oxygen containing contaminant, showing that correlation analysis can be used to complement the standard use of survey spectra to identify contaminants, which we assert should still be carried out in all cases.

Lastly, if the phase model is not known, correlations can be used to gain some insight of the functional groups or chemical environments possible. This is the most challenging application and is helped by input from other analytical methods wherever possible.

There are several assumptions we have made. We assume that the compositions obtained from XPS peak area analysis are accurate, and this implies the relative sensitivity factors (RSFs) are correct. Correlations may occur by chance and not due to underlying chemistry. We assume that chemical environments that occur in the same phase will have constant binding energy separation. This would benefit from further testing on a wider range of samples.

We believe correlation analysis, and the use of phase models, will assist analysis of complex XPS datasets.

4. Experimental section

X-ray photoelectron spectroscopy (XPS) was carried out in a Thermo NEXSA spectrometer. The instrument utilized a 72 W monochromated Al Kα X-ray source (E=1486.6 eV) focused to a spot of 400 μm diameter at the sample surface. Charge compensation was accomplished by use of a dual beam (electron and Ar^+ ion) flood gun. The electron energy analyser consisted of a double focusing 180° hemisphere with mean radius 125 mm, operated in constant analyser energy (CAE) mode, and a 128 channel position sensitive detector. The pass energy was set to 200 eV for survey scans and 40 eV for high resolution regions. The binding energy scale of the instrument is regularly calibrated using a three-point energy reference (Ag, Au, Cu). No calibration of the BE scale was carried out (e.g. by alignment of C 1*s* to a particular BE value). Samples were immobilized on conductive carbon tape for analysis. Stability was assessed by time-resolved measurements of the core lines; no changes were observed indicating that beam damage was not detectable on the time scale of these experiments. Ar ion etching was carried out using a mono Ar^+ ion gun with beam energy of 2000 eV rastered over a 4 mm^2 area of the sample. Where area scans were carried out, a rectangular grid of regularly spaced points were measured. Data was processed in Thermo Avantage software.

4.1. Glossary

Correlation analysis: the plotting of either the atomic % of the binding energy of two elements against each other over a dataset consisting of many sets of spectra taken on the same system. Correlation analysis considers an underlying phase model and compares the expected correlations from that model with those seen experimentally. This can be used to identify which phases are present, or to validate peak fitting models used in XPS to quantify different chemical environments.

Phase: A region with a fixed chemical composition, and within which the elements experience uniform variation in electrical potential relative to the spectrometer. Elements within a phase have a fixed ratio, and core lines from elements in the same phase are assumed to have constant difference in binding energy.

Phase model: A proposed collection of phases that are present in a system. This is a physical model that underlies the understanding of correlation graphs. A phase model allows the proportion of each phase to vary (including to zero).

Dataset: A collection of spectra from the same system. Depth profiles, area maps, time resolved spectra are examples of different kinds of datasets.

System: A sample or samples to which one phase model applies. This may be a single sample or a collection of samples, as long as they can be described well by the same phase model.

Phase fraction: the molar proportion of a phase present, expressed as a percentage.

Isoelemental phases: phases that share one or more common elements. The opposite is anioselemental phases that do not share any common elements. The concept can be broadened by the ability of XPS to distinguish chemical environments of the same element. If an accurate peak fitting model of chemical states can be applied to the core line spectra, then the chemical environments may be quantified separately and isoelemental phases may be able to be treated as anisoelemental phases for correlation analysis.

Tie line: a line on an atomic % correlation graph that links the points where X_A=0% and X_A=100 %.

CRediT authorship contribution statement

Prajna Bhatt: Writing – review & editing, Methodology, Data curation. **Mark Isaacs:** Writing – review & editing, Methodology, Data curation. **Yuhan Liu:** Writing – review & editing, Methodology, Data curation. **Robert G. Palgrave:** Conceptualization, Methodology, Writing - original draft, Supervision, Funding acquisition.

Declaration of competing interest

The authors declare the following financial interests/personal relationships which may be considered as potential competing interests: Yuhan Liu reports financial support was provided by China Scholarship Council. If there are other authors, they declare that they have no known competing financial interests or personal relationships that could have appeared to influence the work reported in this paper.

Acknowledgements

Y.L. acknowledges funding from the China Scholarship Council. XPS was carried out at HarwellXPS, the National XPS Facility (EP/Y023587/1). The authors thank Aisha Mumtaz, David Morgan and Tim Nunney for helpful discussions.

Appendix A. Supplementary data

Supplementary data to this article can be found online at https://doi.org/10.1016/j.apsusc.2024.160808.

References

[1] D.N.G. Krishna, J. Philip, Review on surface-characterization applications of X-ray photoelectron spectroscopy (XPS): Recent developments and challenges, Appl. Surf. Sci. Adv. 12 (2022).

[2] M.A. Isaacs, J. Davies-Jones, P.R. Davies, S.L. Guan, R. Lee, D.J. Morgan, R. Palgrave, Advanced XPS characterization: XPS-based multi-technique analyses for comprehensive understanding of functional materials, Mater. Chem. Front. 5 (22) (2021) 7931–7963.

[3] P.S. Bagus, E. Ilton, C.J. Nelin, Extracting chemical information from XPS spectra: a perspective, Catal. Lett. 148 (7) (2018) 1785–1802.

[4] G.H. Major, V. Fernandez, N. Fairley, E.F. Smith, M.R. Linford, Guide to XPS data analysis: Applying appropriate constraints to synthetic peaks in XPS peak fitting, J. Vac. Sci. Technol. A 40 (6) (2022).

[5] A.G. Shard, Practical guides for x-ray photoelectron spectroscopy: Quantitative XPS, J. Vac. Sci. Technol. A 38 (4) (2020).

[6] G.H. Major, T.G. Avval, B. Moeini, G. Pinto, D. Shah, V. Jain, V. Carver, W. Skinner, T.R. Gengenbach, C.D. Easton, A. Herrera-Gomez, T.S. Nunney, D.R. Baer, M. R. Linford, Assessment of the frequency and nature of erroneous x-ray photoelectron spectroscopy analyses in the scientific literature, J. Vac. Sci. Technol. A 38 (6) (2020).

[7] G. Greczynski, L. Hultman, X-ray photoelectron spectroscopy: Towards reliable binding energy referencing, Prog. Mater Sci. 107 (2020) 100591.

[8] G.H. Major, N. Farley, P.M.A. Sherwood, M.R. Linford, J. Terry, V. Fernandez, K. Artyushkova, Practical guide for curve fitting in x-ray photoelectron spectroscopy, J. Vac. Sci. Technol. A 38 (6) (2020).

[9] P.S. Bagus, C.J. Nelin, C.R. Brundle, Chemical significance of x-ray photoelectron spectroscopy binding energy shifts: a perspective, J. Vac. Sci. Technol. A 41 (6) (2023).

[10] S. Tougaard, Energy loss in XPS: fundamental processes and applications for quantification, non-destructive depth profiling and 3D imaging, J. Electron Spectrosc. Relat. Phenom. 178–179 (2010) 128–153.

[11] T.G. Avval, N. Gallagher, D. Morgan, P. Bargiela, N. Fairley, V. Fernandez, M. R. Linford, Practical guide on chemometrics/informatics in x-ray photoelectron spectroscopy (XPS). I. Introduction to methods useful for large or complex datasets, J. Vac. Sci. Technol. A 40 (6) (2022).

[12] T.G. Avval, H. Haack, N. Gallagher, D. Morgan, P. Bargiela, N. Fairley, V. Fernandez, M.R. Linford, Practical guide on chemometrics/informatics in x-ray photoelectron spectroscopy (XPS). II. Example applications of multiple methods to the degradation of cellulose and tartaric acid, J. Vac. Sci. Technol. A 40 (6) (2022).

[13] A. Machida, K. Nagata, R. Murakami, H. Shinotsuka, H. Shouno, H. Yoshikawa, M. Okada, Bayesian estimation for XPS spectral analysis at multiple core levels, Sci. Technol. Adv. Mater.: Methods 1 (1) (2021) 123–133.

[14] J.M. Kahk, J. Lischner, Core electron binding energies of adsorbates on Cu(111) from first-principles calculations, PCCP 20 (48) (2018) 30403–30411.

[15] D. Golze, L. Keller, P. Rinke, Accurate Absolute and Relative Core-Level Binding Energies from GW, J. Phys. Chem. Lett. 11 (5) (2020) 1840–1847.

[16] J.M. Pi, M. Stella, N.K. Fernando, A.Y. Lam, A. Regoutz, L.E. Ratcliff, Predicting core level photoelectron spectra of amino acids using density functional theory, J. Phys. Chem. Lett. 11 (6) (2020) 2256–2262.

[17] A. Regoutz, M.S. Wolinska, N.K. Fernando, L.E. Ratcliff, A combined density functional theory and x-ray photoelectron spectroscopy study of the aromatic amino acids, Electr. Struct. 2 (4) (2020) 044005.

[18] V. Fernandez, D. Morgan, P. Bargiela, N. Fairley, J. Baltrusaitis, Combining PCA and nonlinear fitting of peak models to re-evaluate C 1s XPS spectrum of cellulose, Appl. Surf. Sci. 614 (2023) 156182.

[19] P.D. Harrington, A. Urbas, P.J. Tandler, Two-dimensional correlation analysis, Chemom. Intel. Lab. Syst. 50 (2) (2000) 149–174.

[20] C. Kalha, N. Fernando, A. Regoutz, Digitisation of Scofield Photoionisation Cross Section Tabulated Data, Figshare (2020).

[21] J.H. Scofield, Theoretical photoionization cross sections from 1 to 1500 keV, United States (1973) 376.

[22] D. Fang, F. He, J.L. Xie, L.H. Xue, Calibration of Binding Energy Positions with C1s for XPS Results, J. Wuhan Univ. Technol.-Mater. Sci. Ed. 35 (4) (2020) 711–718.

[23] G. Greczynski, L. Hultman, C1s Peak of Adventitious Carbon Aligns to the Vacuum Level: Dire Consequences for Material's Bonding Assignment by Photoelectron Spectroscopy, ChemPhysChem 18 (12) (2017) 1507–1512.

[24] K.M.G. Siegbahn, W.C. Price, D.W. Turner, A Discussion on photoelectron spectroscopy - Electron spectroscopy for chemical analysis, (e.s.c.a.) 268 (1184) (1970) 33–57.

[25] J. Cazaux, Mechanisms of charging in electron spectroscopy, J. Electron Spectrosc. Relat. Phenom. 105 (2) (1999) 155–185.

[26] T. Stamenković, N. Bundaleski, T. Barudžija, I. Validžić, V. Lojpur, XPS study of iodine and tin doped Sb2S3 nanostructures affected by non-uniform charging, Appl. Surf. Sci. 567 (2021) 150822.

[27] E.N.K. Glover, S.G. Ellington, G. Sankar, R.G. Palgrave, The nature and effects of rhodium and antimony dopants on the electronic structure of TiO2: towards design of Z-scheme photocatalysts, J. Mater. Chem. A 4 (18) (2016) 6946–6954.

[28] A. Klein, K. Albe, N. Bein, O. Clemens, K.A. Creutz, P. Erhart, M. Frericks, E. Ghorbani, J.P. Hofmann, B. Huang, B. Kaiser, U. Kolb, J. Koruza, C. Kübel, K.N. S. Lohaus, J. Rödel, J. Rohrer, W. Rheinheimer, R.A. De Souza, V. Streibel, A. Weidenkaff, M. Widenmeyer, B.-X. Xu, H. Zhang, The Fermi energy as common parameter to describe charge compensation mechanisms: A path to Fermi level engineering of oxide electroceramics, J. Electroceram. 51 (3) (2023) 147–177.

[29] A. Klein, C. Körber, A. Wachau, F. Säuberlich, Y. Gassenbauer, S.P. Harvey, D. E. Proffit, T.O. Mason, Transparent Conducting Oxides for Photovoltaics: Manipulation of Fermi Level, Work Function and Energy Band Alignment, Materials (basel, Switzerland) 3 (11) (2010) 4892–4914.

[30] D. Briggs, M.P. Seah, Practical surface analysis : by Auger and x-ray photoelectron spectroscopy / edited by D, Briggs and M.P. Seah. Wiley, Chichester, 1983.

[31] C.L. Lau, G.K. Wertheim, Oxidation of tin: an ESCA study, J. Vac. Sci. Technol. 15 (2) (1978) 622–624.

[32] M.A. Stranick, A. Moskwa, SnO2 by XPS, Surf. Sci. Spectra 2 (1) (1993) 50–54.

[33] G. Silversmit, D. Depla, H. Poelman, G.B. Marin, R. De Gryse, Determination of the V2p XPS binding energies for different vanadium oxidation states (V⁵⁺ to V⁰⁺), J. Electron Spectrosc. Relat. Phenom. 135 (2–3) (2004) 167–175.

[34] M. Smith, L. Scudiero, J. Espinal, J.-S. McEwen, M. Garcia-Perez, Improving the deconvolution and interpretation of XPS spectra from chars by ab initio calculations, Carbon 110 (2016) 155–171.

[35] P. Louette, F. Bodino, J.-J. Pireaux, Poly(vinyl alcohol) (PVA) XPS Reference Core Level and Energy Loss Spectra, Surf. Sci. Spectra 12 (1) (2007) 106–110.

[36] G. Beamson, A. Bunn, D. Briggs, , High-Resolution Monochromated XPS of Poly (methyl Methacrylate) Thin Films on a Conducting Substrate. 17 (2) (1991) 105–115.

[37] X.M. Zeng, C.M. Chan, L.T. Weng, L. Li, Surface characterization and quantitative study of poly(4-vinyl phenol) and poly(4-vinyl pyridine) blends by XPS and ToF-SIMS, Polymer 41 (23) (2000) 8321–8329.